Structure parameters and magnetic properties of nanosized strontium hexaferrite prepared by the sol-gel combustion method

2017 IOP Conf. Ser.: Mater. Sci. Eng. 168 012075

(http://iopscience.iop.org/1757-899X/168/1/012075)

Structure parameters and magnetic properties of nanosized strontium hexaferrite prepared by the sol-gel combustion method

V A Zhuravlev[1], R M Minin[2], V I Itin[2], M V Politov[1], I Yu Lilenko[1] and M R Ufimtsev[1]

[1]Tomsk State University, Lenin av., 36, Tomsk, 634050 Russia
[2] Tomsk Scientific Center SB RAS, pr. Academicheskii 10/4, Tomsk, 634021 Russia

E-mail: ptica@mail.tsu.ru

Abstract. The phase composition, structure parameters, and main magnetic characteristics of $SrFe_{12}O_{19}$ hexaferrite prepared by the sol-gel combustion method in combination with subsequent annealing at the temperature of 850°C for 6 hours are investigated. From the study of the magnetization curves in the pulsed magnetic fields the value of saturation magnetization of synthesized material was determined. The value of the magnetocrystalline anisotropy field was determined from the survey of the ferromagnetic resonance.

1. Introduction

Hexagonal ferrite of M-type $SrFe_{12}O_{19}$ is characterized by a large coercive force, comparatively large value of the saturation magnetization, high Curie temperature, large magnetocrystalline anisotropy, high electric resistance, high chemical stability and corrosion resistance. Due to the qualities listed and its low cost the ferrite is used in different spheres of science and technology as permanent magnets and bonded magnets, in various microwave devices (circulators, isolator, phase shifters, filters) and in magnetic and magneto-optic recorders of information with high density [1]. For the reasons listed above the materials which possess the controllable size and form of particles, narrow distribution of particles according to the size and with given magnetic characteristics are needed.

The traditional ceramic method of strontium hexaferrite synthesis is burning the mixture of $SrCO_3$ and Fe_2O_3 powders at a high temperature (> 1200 °C). The disadvantages of this method are high power consumption, uncontrolled morphology of particles, chemical heterogeneity and big size of particles and their agglomerates. Grinding of synthesized strontium hexaferrite powder leads to admixtures, elastic stresses and worsening of magnetic properties [2, 3].

To control the size and form of the particles as well as the magnetic properties of materials new energy-saving methods have been suggested. Such as sol-gel method and its modifications [4, 5], pyrolysis of aerosol, coprecipitation, hydrothermal method, SHS etc. The full description of these methods can be found in the review [1]. As a rule, using these methods the nanosized and nanostructured particles are obtained which possess the properties different from the properties of massive polycrystalline materials due to the significant part of atoms present in the defective surface layer. By means of additional annealing one can change the size of particles, their morphology and the magnetic properties.

In the present work, the sol-gel combustion method is used to prepare nanosized strontium hexaferrite powders of M-type with the $SrFe_{12}O_{19}$ composition. The method is based on the preparation of initial colloid nanosystem that can react in the combustion mode. This method is the most suitable for the preparation of powder materials with good stoichiometric control, narrow particle size distribution and it requires relatively short processing time at lower temperatures [6]. Results of investigations the phase composition, structural parameters, and magnetic properties of the synthesized materials are presented.

Research of the magnetocrystalline anisotropy of the samples was carried out by the method of ferromagnetic resonance (FMR). FMR is the only method for the study of the magnetocrystalline anisotropy of the multi-phase powder samples consisting of a phases with significantly different values of the anisotropy fields [7].

2. Preparation of samples

As the reagents the aqueous solutions of analytical grade strontium nitrate $Ba(NO_3)_2$, analytical grade 9-aqueous iron nitrate $Fe(NO_3)_3 \cdot 9H_2O$, and lemon acid $C_6H_8O_7$ with concentration of 1 M were mixed in proportions

$$\{[\ Sr(NO_3)_2]:[\ Fe(NO_3)_3 \cdot 9H_2O]\}:C_6H_8O_7 = \{1:11.5\}:2.$$

The concentrated solution of NH_4OH ammonium hydroxide was added dropwise to the prepared mixture with constant stirring until pH of the solution became equal to 7. An HI98103 checker portable digital tester (HANNA Instruments) was used to measure pH of the solution mixture. The prepared sol was heated in an ES-6120 magnetic stirrer (EKROS) at temperatures from 80 to 90°C for 3–5 h. As a result of heating, the sol was transformed into a viscous gel of brown color which foamed. Further heating of the gel foam to temperatures 150–160°C caused its ignition and combustion that lasted for several minutes. After combustion, a friable powder was obtained which was easily grinded in a mortar converting into a fine powder. The $SrFe_{12}O_{19}$ hexaferrite nanoparticles were finally formed by annealing of the powder at the temperature of 850°C for 6 h.

3. The research techniques

The X-ray diffraction analysis was performed with a SHIMADZU XRD-6000 polycrystalline diffractometer in the Bragg–Brentano geometry with a focusing pyrographite crystal-monochromator inserted into the secondary gamma-quantum beam. For qualitative analysis of the phase composition, the PDF4+ computer database of x-ray powder diffractometry of the International Center of Diffraction Data (ICDD, Denver, USA) was used. The quantitative analysis of the phase composition and the refinement of the structural parameters of the detected phases were performed using the Powder Cell 2.4 program of full profile analysis. The infrared spectrum was registered with a Nicolet 5700 infrared Fourier spectrometer (France) equipped with an attachment of diffuse reflection.

Magnetic measurements involved investigations of magnetization curves in pulsed magnetic fields up to 30 kOe using a setup described in [8] and measurements of ferromagnetic resonance (FMR) spectra by the standard waveguide passing through technique at frequencies in the range 37–53 GHz with an automated radio spectroscope. To investigate the FMR, powders of the examined samples were put in thin-walled quartz tubes with inner diameter of 0.7 mm and length of 10 mm. The tubes were arranged into a rectangular waveguide parallel to the wide wall of the waveguide in order that the alternating magnetic field was directed along the sample axis. A constant magnetizing field was directed perpendicularly to the wide wall of the waveguide.

4. The results of x-ray researches

The X-ray diffraction patterns of the synthesis product after ferritization at 850 °C for 6 hours are shown in Fig. 1. It can be seen that it contains basically diffraction peaks corresponding to $SrFe_{12}O_{19}$ hexaferrite. The traces of accompanying hematite phase (α-Fe_2O_3) are also present.

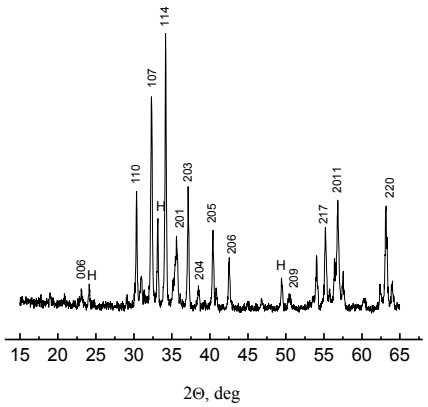

Figure 1. X-ray diffraction pattern of $SrFe_{12}O_{19}$ hexaferrite powder synthesized by sol-gel combustion method. The letters H show the traces of the hematite phase.

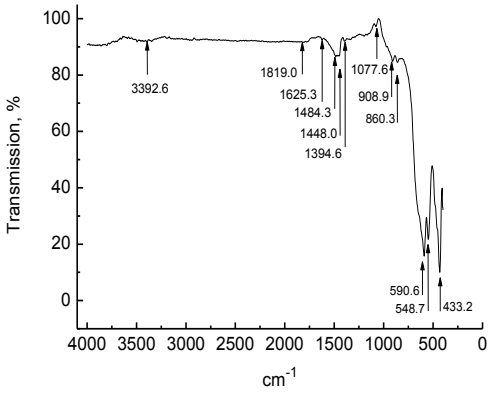

Figure 2. IR-spectrum of product after sol-gel combustion and heat treatment at 850 °C for 6 hours.

Results of the x-ray diffraction analysis of the sample are given in Table 1.

Table 1. Phase composition and structural parameters of synthesized material after calcinations.

Phase constitution, %		Lattice constant, Å		CSR, nm	$\Delta d/d*10^3$
$SrFe_{12}O_{19}$	α-Fe_2O_3	*a*	*c*		
99.4	0.6	5.9175	23.3130	98	2.7

The content of the Sr–M main phase exceeded 99% and hematite α-Fe_2O_3 was the additional phase. The average crystallite sizes (~ 100 nm) were estimated based on an analysis of the physical broadening of diffraction lines from sizes of coherent scattering region (CSR). In the last column of the Table 1 shown the relative changes in the interplanar distances $\Delta d/d$. The estimates of internal elastic microstrain $\sigma = E(\Delta d/d)$ can be carried out by that. Here E – Young's modulus.

5. FTIR spectrum of the sample

The Figure 2 shows the infrared spectrum of transmission coefficient of the obtained hexaferrite powder after annealing at T = 850 °C for 6 hours. At frequencies in the range 3500–3300 cm^{-1}, a very weak absorption band caused by strain-induced vibrations of O–H groups is observed, wide in comparison with other bands. It corresponds with a weak absorption band at 1625 cm^{-1} caused by H–O–H vibrations (bending vibrations of water molecules). The bands at 1484 - 1448 cm^{-1} and 860 cm^{-1} are due to the C–O vibrations due to the presence of lemon acid residues in the water.

The band localized at 909 cm^{-1} is probably attributed to the impurity phase α-Fe_2O_3 which corresponds with the data of X-ray diffraction analysis (Table 1). The bands observed at 433, 549 and 591cm^{-1} can be attributed to valence vibrations metal-oxygen of strontium hexaferrite. Similar results were obtained in [4] for strontium hexaferrite, synthesized by sol-gel combustion method with the usage of egg white.

Thus, the X-ray diffraction and spectrometric data given above prove that the synthesized material is strontium hexaferrite $SrFe_{12}O_{19}$.

6. Research of the magnetization curves

A study of the magnetization curves of $SrFe_{12}O_{19}$ hexaferrite powder was conducted at the room temperature in the pulsed magnetic field by the method described in [8]. The results are presented in the Figure 3. The arrows show the direction of the magnetizing field alteration. The linear

extrapolation of high-field part of the magnetization curves on the zero magnetizing fields gives the estimation for the specific saturation magnetization (σ_s). The specific residual magnetization (σ_r) can be determined from the point of intersection of the drop-down portion of the magnetization curve with the Y-axis.

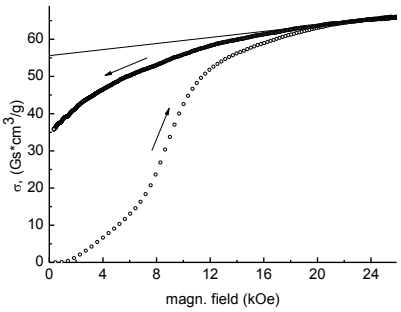

Figure 3. The magnetization curve of the synthesized strontium hexaferrite powder. The arrows show the direction of the magnetizing field alteration.

The values of the specific residual magnetization (σ_r) and the specific saturation magnetization (σ_s) are presented in the first row of the Table 2. In the last column of the table the calculations according to the formula $M_S = \sigma_S \cdot \rho$ are shown. Here $\rho = 5.11$ g/cm^3 is the density of strontium hexaferrite [1]. In the subsequent rows of the table for comparison are presented the results obtained in other studies.

Table 2. The research results of the magnetization curves

Sample	σ_r, Gs·cm^3/g	σ_s, Gs·cm^3/g	σ_r / σ_s	Size, nm	M_S, Gs
Sol-gel combustion, 850 °C	35.9	55.8 (0 kOe)	0.64	~ 100	285
Sol-gel [4], 1200 °C	-	56.2 (10 kOe)	-	≥ 1000	-
Sol-gel [5], 825 °C	-	62.6 (15 kOe) 70.8 (50 kOe)	0.49	135x50	-
Sol-gel [1], 1000-1200 °C	-	56 ÷ 70	-	-	-

In the paper [4] where the egg white was used as a fuel the value of σ_s measured in the field ~10 kOe is close to the one obtained in this study though the sizes of the particles differ significantly due to the different temperature of annealing. In the paper [5] the modified sol-gel synthesis is used and the hexaferrite particles were formed and annealed in the NaCl matrix. So a big value for the specific saturation magnetization was obtained. The data from the review [1] are given in the line 4 of the table. It is clear that the above values of σ_s are typical for strontium hexaferrites that synthesized by the sol-gel methods.

7. The study of the magnetic anisotropy by the FMR method

The study of ferromagnetic resonance spectrum for powder and polycrystalline hexaferrites gives an opportunity to experimentally determine the values and the sign of the fields of magnetocrystalline anisotropy (H_{ai}) as well as the value of the gyromagnetic ratio $\gamma = ge/2mc$, where g is the effective g-factor of the examined material, e is the electron charge, m is the electron mass, and c is the velocity of light. It has to be noted that in hexaferrites the γ parameter can be anisotropic [9]. The magnitudes and signs of the anisotropy fields H_{ai} define the type of magnetic ordering – the presence of either an easy magnetization plane (EMP) or an easy magnetization axis (EMA).

The method described in [9, 10] was used to calculate the resonance curves of FMR or components of permeability tensor of the single-domain polycrystalline and powder ferrimagnets with hexagonal crystal structure in the approach of non-interacting grains. The calculations showed:

- The shape of FMR curves makes it possible to define what type of anisotropy the material has: an EMA or an EMP.
- The resonance curves or field dependences of the imaginary parts of components the permeability tensor have two features: maximums and (or) steps. The low-field feature is caused by the resonance of crystallites in which the direction of the magnetic field ($\vec{H}$) is close to the direction of easy magnetization. The high-field feature corresponds to the resonance of the crystallites in which the field is oriented near the hard magnetization directions.

The features on the FMR curves are observed close to the values of the magnetizing fields which correspond to the stationary directions on the angular dependence of resonance field: $H_{\parallel}$ and $H_{\perp}$. The stationary directions are the maxima and minima on an angular dependence of the resonance field of monocrystalline grains. The values of these resonance fields (or frequencies) are determined by the formulas [10]:

$$\omega_{\parallel} = \gamma_{\parallel}\left[H_{\parallel} + (\gamma_{\perp}/\gamma_{\parallel})H'_{a1}\right], \quad \omega_{\perp} = \gamma_{\perp}\left[H_{\perp}\left(H_{\perp} - H_{\theta}\right)\right]^{1/2}. \tag{1}$$

Here $\omega_{\parallel}$, $\gamma_{\parallel}$ and $\omega_{\perp}$, $\gamma_{\perp}$ are resonance frequencies and gyromagnetic ratios for directions along the hexagonal axis *c* of the crystalline lattice and in the base plane, H'_{a1}, H_{θ} are the magnetocrystalline anisotropy fields for these directions. These fields include contributions from magnetocrystalline anisotropy and anisotropy of the shape of crystallite:

$$H_{\theta} = H'_{a1} + H_{a2} + H_{a3}, \; H'_{a1} = H_{a1} + 4\pi M_S(N_{\perp} - (\gamma_{\perp}/\gamma_{\parallel})^2 N_{\parallel}). \tag{2}$$

In the formulas (2) $H_{ai} = 2ik_i/M_S$ are the fields of magnetocrystalline anisotropy (i = 1, 2, 3); $N_{\perp}$, $N_{\parallel}$ are demagnetizing factors of the particle that has a form of ellipsoid of revolution, $2N_{\perp} + N_{\parallel} = 1$.

Figure 4 shows the experimental resonance curves (points) of the sample Sr-M, measured in three frequencies. In the range of magnetizing fields to 23 kOe one maximum is observed in the field close to $H_{\parallel}$, which corresponds with the direction of EMA. With the decrease of frequency the maxima shift to the smaller fields. The increase of losses in zero fields with the decrease of frequency is defined by the approach of the high-frequency magnetic field to the frequency of natural ferromagnetic resonance which is defined by the formula:

$$\omega_{NFMR} = \gamma_{\perp} H'_{a1}. \tag{3}$$

According to the Fig. 4, for the Sr-M hexaferrite this frequency is $\omega_{NFMR} \approx 2\pi$*48 GHz.

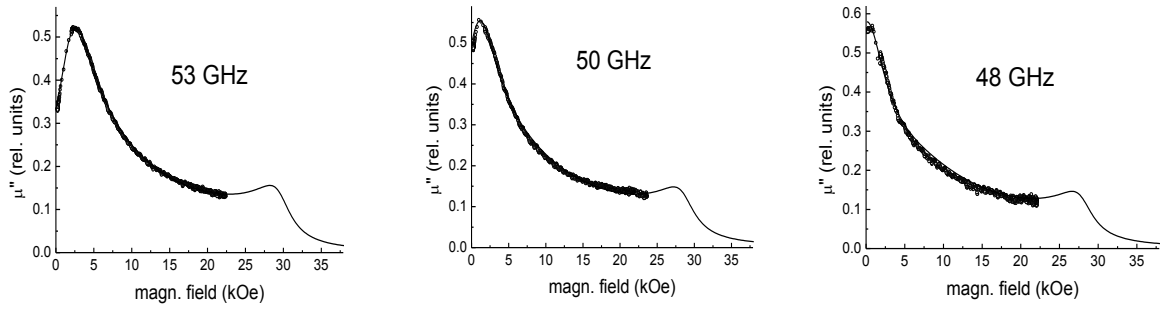

Figure 4. Curves of FMR Sr-M sample measured at different frequencies. The calculated curves are represented by lines, experimental data are represented by points.

The processing of experimental FMR spectra was carried out in two stages. In the first stage, the frequency dependences of the resonance fields were drawn. Then the estimations for magnetomechanical ratios γ and anisotropy fields (H'_{a1}) were performed by the least squares method for $\omega_{\parallel}$ according to the formula 1. At the second stage, more accurate values of these parameters were

determined by a detailed comparison of the shapes of experimental and calculated resonance curves at different frequencies. In the resonance curves calculations the gyromagnetic ratio was considered to be isotropic $\gamma_{\parallel} = \gamma_{\perp} = \gamma$, and the value of anisotropy field $H_{\theta} = H_{a1}^{'}$.

The calculated imaginary parts of the diagonal components of the permeability tensor are represented by lines in Figure 4. The calculated curves in the figure are shown in a wider range of magnetizing field than the experimental points. This is done in order to show a presence another peak near the field corresponding to the direction of hard magnetization ($H_{\perp}$). The resonance curves were calculated for values of γ, $H_{a1}^{'}$, M_S and α, shown in the first row of Table 3. Here, α is a decay constant of monocrystalline grains in the Landau-Lifshitz-Gilbert equation of motion.

Table 3. Parameters of the calculated resonance curves

Sample	CSR, nm	$\gamma/2\pi$, GHz/kOe	$H_{a1}^{'}$, kOe	M_S, Gs	M_r/M_S	α
$SrFe_{12}O_{19}$	98	2.78	17.25	285	0.64	0.12
$BaFe_{12}O_{19}$ [11]	87	2.80	15.40	366	0.58	-

The second row of Table 3 shows the characteristics of barium hexaferrite $BaFe_{12}O_{19}$. This sample was synthesized in [11] with the same procedure as in our work. According to the table, the particle size and the magnitude of the gyromagnetic ratio of strontium and barium hexaferrites of M-type differ slightly. The anisotropy field of hexaferrite Sr-M almost two kOe greater than anisotropy field of the BaM. This is consistent with the data for bulk materials [1]. Therefore, the ratio of M_r/M_S in SrM also higher, indicating the higher value of the coercive force.

8. Conclusion

Thus, the technology of synthesis of Sr-M hexaferrite by sol-gel combustion produces materials with magnetic properties close to the properties of the materials synthesized by conventional ceramic technology. The advantage of the proposed technology is a significant reduction in synthesis time and energy consuming process.

Acknowledgments

This Research is supported by Tomsk State University Competitiveness Improvement Program reg. N 8.1.23.2015

References

[1] Pillar R. C. 2012 *Progress in Material Science* **57** 1191
[2] Ding J, Maurice D, Miao W F, McCormick P G and Street R 1995 *J Magn. Magn. Mater.* **150** 417
[3] Mendoza-Suárez G, Matutes-Aquino J A, Escalante-García J I, Mancha-Molinar H, Ríos-Jara D and Johal K K 2001 *J. Magn. Magn. Mater.* **223** 55
[4] Li T, Li Y, Wu R, Zhou H, Fang X, Su S, Xia A, Jin C and Liu X. 2015 *J. Magn. Magn. Mater.* **393** 325
[5] Sapoletova N A, Kushnir S E, Li Y H, An S Y, Seo J W and Hur K H 2015 *J. Magn. Magn. Mater.* **389** 101
[6] Padampalle A S, Suryawanshi A D, Navarkhele V M and Birajdar D S 2013 *Int. J. of Recent Technology and Engineering* **2** 19
[7] Zhuravlev V A and Naiden E P 2009 *Physics of the Solid State* **51** 327
[8] Kreslin V Yu and Naiden E P 2002 *Prib. Tekh. Eksp.* **1** 63
[9] Zhuravlev V A 1999 *Physics of the Solid State* **41** 956
[10] Zhuravlev V A and Meshcheryakov V A 2014 *Russian Physics Journal* **56** 1387
[13] Naiden E P, Zhuravlev V A, Minin R V, Itin V I, Korovin E Yu 2015 *Russian Physics Journal* **58** 125